European Heart Journal - Cardiovascular Imaging (2017) **18**, 862–869
doi:10.1093/ehjci/jew304

Novel application of 3D contrast-enhanced CMR to define fibrotic structure of the human sinoatrial node *in vivo*

Thomas A. Csepe[1], Jichao Zhao[2], Lidiya V. Sul[1], Yufeng Wang[2], Brian J. Hansen[1], Ning Li[1], Anthony J. Ignozzi[1], Anna Bratasz[1,3], Kimerly A. Powell[1,3], Ahmet Kilic[3,4], Peter J. Mohler[1,3,5], Paul M.L. Janssen[1,3,5], John D. Hummel[3,5], Orlando P. Simonetti[3,6], and Vadim V. Fedorov[1,3]*

[1]Department of Physiology & Cell Biology, The Ohio State University Wexner Medical Center, 304 Hamilton Hall, 1645 Neil Avenue, Columbus, OH 43210, USA; [2]Auckland Bioengineering Institute, The University of Auckland, 70 Symonds Street, Auckland 1142, New Zealand; [3]Davis Heart & Lung Research Institute, The Ohio State University Wexner Medical Center, 473 W 12th Avenue, Columbus, OH 43210, USA; [4]Department of Surgery, The Ohio State University Wexner Medical Center, 410 W 10th Avenue, Columbus, OH 43210, USA; [5]Department of Internal Medicine, The Ohio State University Wexner Medical Center, 395 W 12th Avenue, Columbus, OH 43210, USA; and [6]Department of Biomedical Informatics, The Ohio State University Wexner Medical Center, 250 Lincoln Tower, 1800 Cannon Drive, Columbus, OH 43210, USA

Received 13 August 2016; editorial decision 1 November 2016; accepted 16 November 2016; online publish-ahead-of-print 13 January 2017

Aims The adult human sinoatrial node (SAN) has a specialized fibrotic intramural structure (35–55% fibrotic tissue) that provides mechanical and electrical protection from the surrounding atria. We hypothesize that late gadolinium-enhanced cardiovascular magnetic resonance (LGE-CMR) can be applied to define the fibrotic human SAN structure *in vivo*.

Methods and results LGE-CMR atrial scans of healthy volunteers (*n* olu, 23–52 y.o.) using a 3 Tesla magnetic resonance imaging system with a spatial resolution of 1.0 mm^3 or 0.625 × 0.625 × 1.25 mm^3 were obtained and analysed. Percent fibrosis of total connective and cardiomyocyte tissue area in segmented atrial regions were measured based on signal intensity differences of fibrotic vs. non-fibrotic cardiomyocyte tissue. A distinct ellipsoidal fibrotic region (length: 23.6 ± 1.9 mm; width: 7.2 ± 0.9 mm; depth: 2.9 ± 0.4 mm) in all hearts was observed along the posterior junction of the crista terminalis and superior vena cava extending towards the interatrial septum, corresponding to the anatomical location of the human SAN. The SAN fibrotic region consisted of 41.9 ± 5.4% of LGE voxels above an average threshold of 2.7 SD (range 2–3 SD) from the non-fibrotic right atrial free wall tissue. Fibrosis quantification and SAN identification by *in vivo* LGE-CMR were validated in optically mapped explanted donor hearts *ex vivo* (*n* ivo, 19–65 y.o.) by contrast-enhanced CMR (9.4 Tesla; up to 90 μm^3 resolution) correlated with serial histological sections of the SAN.

Conclusion This is the first study to visualize the 3D human SAN fibrotic structure *in vivo* using LGE-CMR. Identification of the 3D SAN location and its high fibrotic content by LGE-CMR may provide a new tool to avoid or target SAN structure during ablation.

Keywords sinoatrial node • fibrosis • late gadolinium-enhanced CMR • optical mapping • human atria

Introduction

The sinoatrial node (SAN) is the primary pacemaker of the heart and responsible for regulating cardiac rhythm.[1,2] Over 100 years ago, the anatomic structure of the SAN was discovered by Keith and Flack.[3] Since this discovery, animal model and human studies have investigated how cardiac rhythm is initiated and regulated by the SAN.[1–6]

Located along the posterior junction of the superior vena cava (SVC) and the right atrium (RA), the human SAN structure consists of a compact mass of specialized cardiomyocytes enmeshed in a

* Corresponding author. Tel: 1-614-292-9892; Fax: 1-614-292-4888. E-mail: vadim.fedorov@osumc.edu

Table 1 ***In vivo*** **LGE-CMR analysis**

Volunteer	Percent fibrosis (%)												Contrast agent
	2 SD			2.5 SD			3 SD			4 SD			
	SAN	IAS	RAFW	SAN	IAS	RAFW	SAN	IAS	RAFW	SAN	IAS	RAFW	
1A	**46.6**	**23.9**	**0.9**	39.1	13.8	0.1	32.3	7.9	0	17	3.5	0	Magnevist
1B	57.2	52.2	0.3	50.8	28.2	0	**45**	**13**	**0**	31.2	0.3	0	Prohance
2	83.8	66	0.9	67.8	49.1	0	**46.8**	**13.4**	**0**	13.4	1.4	0	Magnevist
3	42.3	37.8	4.5	36.5	18	1.7	**33.4**	**10.1**	**1.0**	26.6	2.1	0	Prohance
4	53.1	32.3	1.6	44	18.7	0.5	**37.9**	**11.2**	**0**	24.3	3.7	0	Prohance
5	**41.6**	**15.7**	**1.4**	28.9	9.8	0	17.9	6.2	0.0	3.2	1.9	0	Prohance
Average	54.1	38.0*	1.6*	44.5	22.9*	0.4*	35.6	10.3*	0.2*	19.3	2.2*	0.0*	
SD	15.8	18.5	1.5	13.6	14.2	0.7	10.5	2.8	0.4	10.2	1.3	0.0	

Bold font indicates the threshold chosen for analysis and presented in figures.
*$P < 0.05$ vs. SAN at the same SD threshold.

dense matrix of collagen and fibroblasts.[1,7,8] The healthy adult human SAN consists of 35–55% fibrotic content that, together with surrounding fatty tissue, provides mechanical and electrical protection from the surrounding atria.[9]

Late gadolinium-enhanced cardiovascular magnetic resonance (LGE-CMR) was originally proposed as a tool for visualizing ventricular scarring and is now a routinely used clinical tool.[10–12] This methodology was later applied to visualize fibrosis and scarring before and after radiofrequency ablation procedures of the left and right atria.[11] Notably, this methodology has never been applied to visualize the normally fibrotic human SAN structure until now. Furthermore, the accurate identification of SAN location may help avoid damaging the SAN and its neurovascular inputs during surgery and targeted ablation procedures. In this study, we utilize LGE-CMR to characterize the human SAN fibrotic structure in healthy volunteers and histologically validated explanted donor hearts.

Methods

Volunteers, without history of cardiac disease (male, $n = 5$, 23–52 y.o., see Supplementary data online, *Table S1*), provided written informed consent as approved by The OSU Institutional Review Board. Explanted human hearts ($n = 5$, see Supplementary data online, *Table S2*) were obtained from Lifeline of Ohio, a non-profit organization that coordinates the donation of human organs, in accordance with The OSU Institutional Review Board.

In vivo LGE-CMR and fibrosis estimation

Volunteers underwent LGE-CMR scans using a 3T MAGNETOM Tim Trio (Siemens HealthCare) with a spatial resolution of 1.0 mm^3 (Volunteers 1 and 3–5) or 0.625 × 0.625 × 1.25 mm^3 (Volunteer 2). LGE-CMR scans were acquired 18–25 min following 0.2 mmol/kg gadolinium agent injection. An electrocardiogram-gated, fat-suppressed 3D inversion recovery gradient recalled echo sequence with respiratory navigator gating was used. Typical scan parameters were as follows: echo time, 2 ms; flip angle, 20°; inversion time, 300 ms; repetition time, 4.4 ms; and receiver bandwidth, 355 Hz/pixel, 8–10 min scan time. 3D image data covering the entire heart including both atria and both ventricles were acquired and reformatted into 2D cross sections (1 mm or 1.25 mm thick, see Supplementary data online, *Table S1*). Volunteer 1 was scanned a second time 1 year later to show the results from a scan with a different contrast agent and is referred to as Volunteer 1B (*Table 1* and *Figure 3*).

From *in vivo* LGE-CMR images, the atrial chamber walls were identified, segmented, smoothed to an isotropic resolution, and volume rendered as a 3D reconstruction using a custom-written Matlab (MathWorks Inc.) program and visualized in 3D using both Matlab and Amira programs (FEI Company) (*Figure 1*). Atrial wall thickness consisted of 2–5 mm except interatrial septum (IAS) and crista terminalis (CT) region.

A patient-specific fibrotic mask was applied to the 3D LGE-CMR atrial structure (see Supplementary data online, *Figure S1*). Signal intensity thresholds at SD above the average right atrial free wall (RAFW) signal intensity, a low-intensity area that served as the signal intensity reference, were considered areas of high intensity post contrast (*Figures 2* and *3*). These areas of high signal intensity were defined as fibrotic tissue in accordance with previously published atrial fibrosis quantification studies using a similar method.[11,13] The heart-specific threshold for SAN LGE fibrosis was selected from within a range, as was done previously,[14] to achieve a percent of fibrotic content within the SAN region consistent with reported values for healthy adult human hearts (35–55%).[6,9] *Table 1* lists fibrosis analysis for thresholds of 2, 2.5, 3, and 4 SD above the RAFW for each volunteer. Subsequently, fibrosis segments were used to distinguish the SAN from surrounding atrial regions by computing a finite difference grid mesh. Regional LGE percentage for the SAN, RAFW, and IAS was calculated by fractionating the area of LGE, based on the applied threshold, from total selected tissue area. 3D fibrosis density maps were constructed at each voxel by determining the percent of neighbouring voxels above the threshold within a 5 pixel radius.

Optical mapping of coronary-perfused *ex vivo* human atria

Explanted human hearts (see Supplementary data online, *Table S2*) were coronary perfused and optically mapped as previously described.[5,6,15] Optical action potentials (OAPs) were recorded by CMOS cameras (100 × 100 pixels, MiCAM Ultima-L, SciMedia Ltd, CA) with 330 μm^2 resolution. All hearts were mapped from the epicardium; moreover, three hearts were also simultaneously mapped from the endocardium using a dual-sided optical mapping system,[15,16] allowing us to obtain simultaneous sub-endocardial and sub-epicardial intramural-weighted OAPs (*Figure 4A and B*). OAPs were analysed using a custom Matlab computer program as previously described.[17] SAN conduction maps as well as atrial

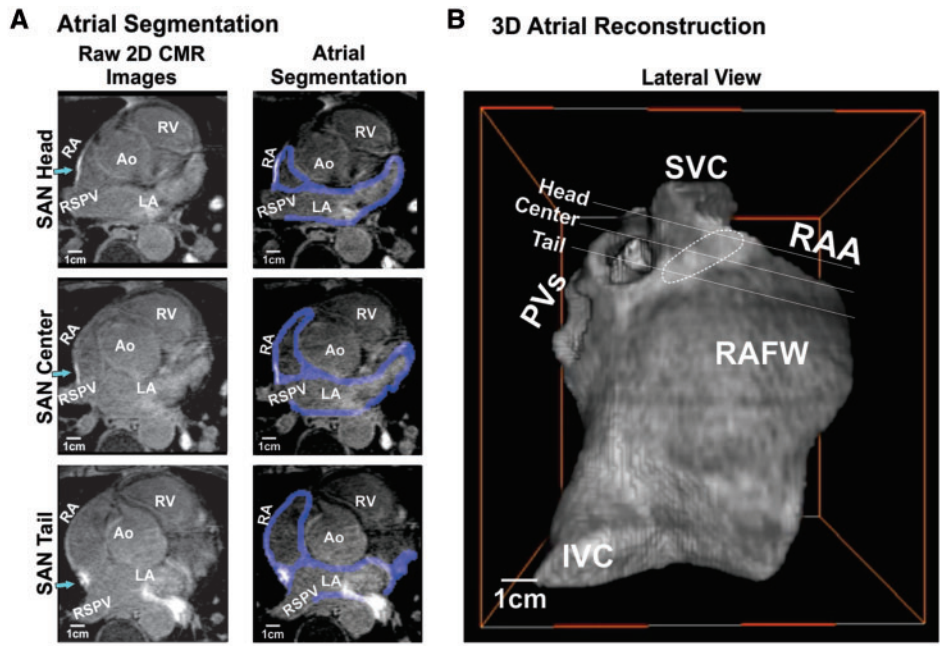

Figure 1 *In vivo* LGE-CMR segmentation and 3D atrial reconstruction. (*A*) 2D imaging cross sections from 3D LGE-CMR SAN head, centre, and tail sections of Volunteer 1A with surrounding atrial tissue. Left: 2D raw images, green arrows point to the SAN head, centre, and tail, respectively; Right: atrial wall segmentation shown in blue. (*B*) 3D atrial reconstruction of the 2D imaging cross sections of Volunteer 1A. Ao, aorta; IVC, inferior vena cava; PVs, pulmonary veins; RA, right atria; RAA, right atrial appendage; RSPV, right superior pulmonary vein; RV, right ventricle; SAN, sinoatrial node; SVC, superior vena cava.

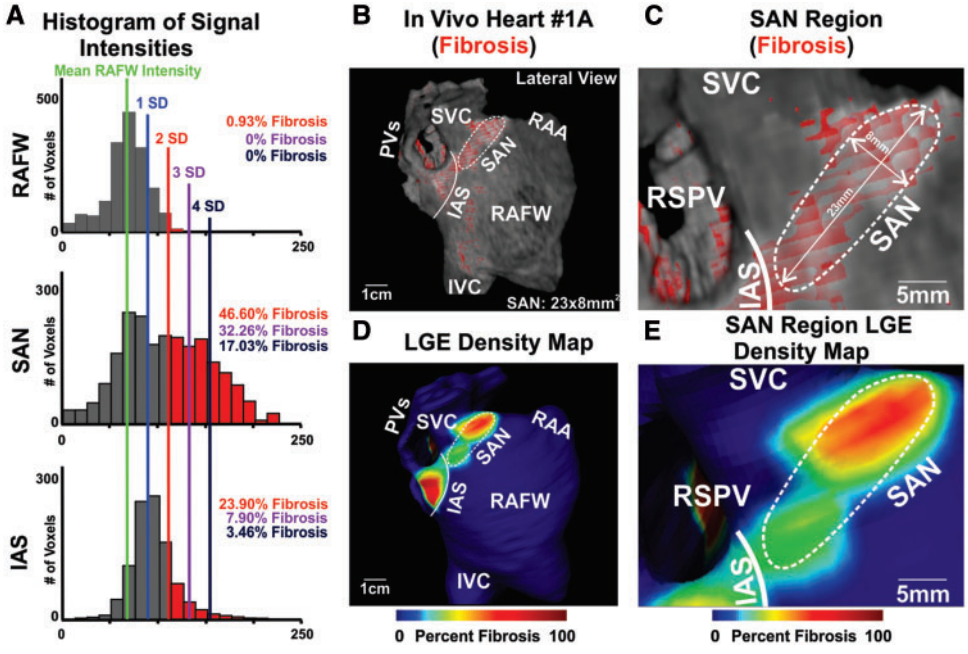

Figure 2 3D SAN fibrotic structure identification by LGE-CMR. (*A*) Signal intensity histograms showing total signal greater than 2 SD above RAFW intensity labelled as fibrosis for Volunteer 1A in panel *B*, percent fibrosis is represented in corresponding colors to SD lines on histograms. (*B*) Lateral view of Volunteer 1A 3D atrial reconstruction with fibrosis enhancement mask (red), white dashed outline showing SAN region, and white solid line showing IAS border. (*C*) Enhanced view of SAN region of 3D atrial reconstruction. (*D*) Lateral view of LGE density map of Volunteer 1A. (*E*) Enhanced view of SAN region of LGE density map. IAS, interatrial septum; IVC, inferior vena cava; PVs, pulmonary veins; RAA, right atrial appendage; RAFW, right atrial free wall; RSPV, right superior pulmonary vein; SAN, sinoatrial node; SVC, superior vena cava.

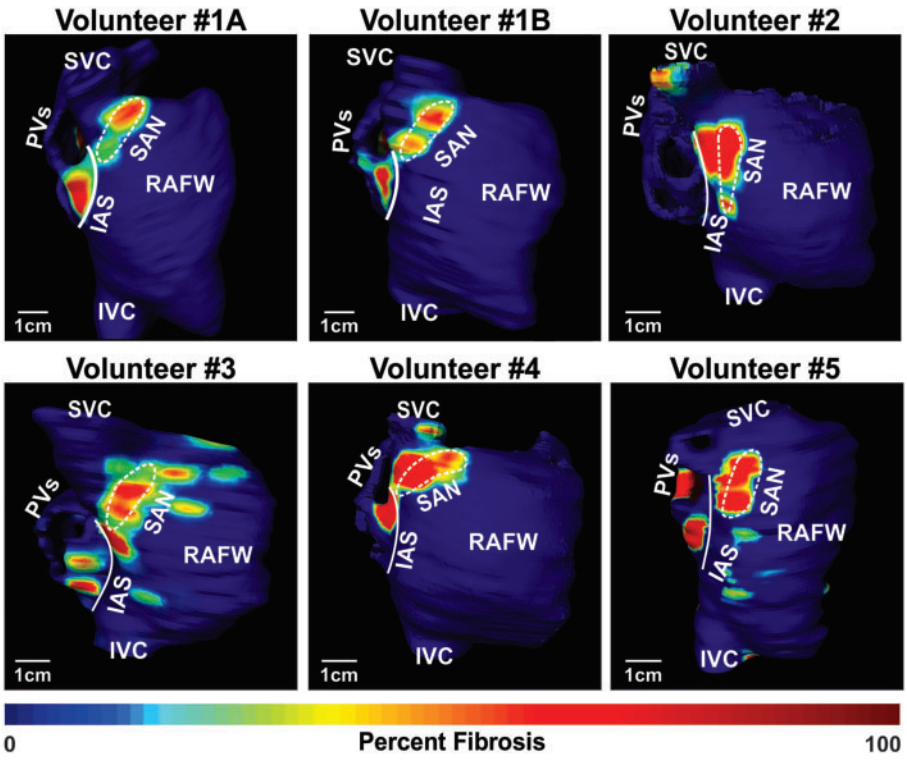

Figure 3 *In vivo* SAN identification by LGE-CMR. 3D atrial reconstructions of fibrotic tissue density of all volunteers. In Volunteer 1, enhanced regions are observed in similar locations in the first scan (top left) and the second scan (top middle), which was performed over 1 year after the initial scan. IAS, interatrial septum; IVC, inferior vena cava; PVs, pulmonary veins; RAFW, right atrial free wall; SVC, superior vena cava.

breakthroughs detected by optical mapping were used to guide SAN dissection for histological sectioning (*Figure 5*). Further details regarding optical mapping of *ex vivo* hearts may be found in the Supplementary data online, *Supplementary Data*.

Ex vivo contrast-enhanced CMR of optically mapped atria with histological validation of fibrosis

Following optical mapping, contrast-enhanced CMR (CE-CMR) was performed on atrial preparations as previously described.[15] 2D CMR images of the SAN with up to 90 μm^2 resolution (*Figure 5* and see Supplementary data online, *Table S2*) were segmented and smoothed using the protocol described for *in vivo* LGE-CMR. After the CE-CMR, SAN regions were sectioned from epicardial to endocardial surfaces at a step of 10 μm thickness for Masson's trichrome staining to validate fibrotic tissue. Histology was used, in addition to optical mapping, to identify and delineate the border of the SAN pacemaker tissue from the surrounding RA based on connexin 43 negativity on immunostaining, distinct cell morphology, clear fibrotic/fat border, and percent tissue fibrosis (see Supplementary data online, *Figure S2*), as previously described in detail.[2,6,7,16,18] Dissection locations based on functional location of SAN were across the SAN pacemaker complex, consisting of the superior (head), middle (centre), and inferior (tail) thirds of the compact node and sinoatrial conduction pathways, which provide a discrete and continuous electrical connection between the SAN and RA (*Figure 4*).[19] SAN sections also included surrounding atrial tissue of the CT, RAFW, and IAS (*Figures 4 and 5* and see Supplementary data online, *Figures S1* and *S2*). 2D histological images with 0.5 × 0.5 μm^2 resolution were analysed in Image J (National Institutes of Health) by colour-based threshold for fibrotic content and compared with corresponding 2D re-sliced CE-CMR cross sections from the same location (see Supplementary data online, *Figure S2*). The series of 2D CE-CMR images were analysed to obtain the optimal fibrosis threshold value best matching the corresponding histological section using a least square approximation. This fibrosis threshold was then applied to the global 3D CE-CMR to perform regional fibrosis analysis of SAN, IAS, CT, and RAFW.

Statistical analysis

Data are presented as mean ± SD. Percent of voxels above fibrosis threshold was compared between the SAN and atrial regions by Student's *t*-test using IBM SPSS Statistics. The correlation between regional percent of fibrotic tissue defined by *ex vivo* CE-CMR and histology is reported as a Pearson correlation coefficient. A value of $P < 0.05$ was considered significant.

Results

In vivo LGE-CMR

In all volunteers, a region of increased continuous fibrotic content at the posterior junction of the SVC and the CT, which is the anatomic location of the SAN,[1] was identified (*Figure 3*). In this region, the head

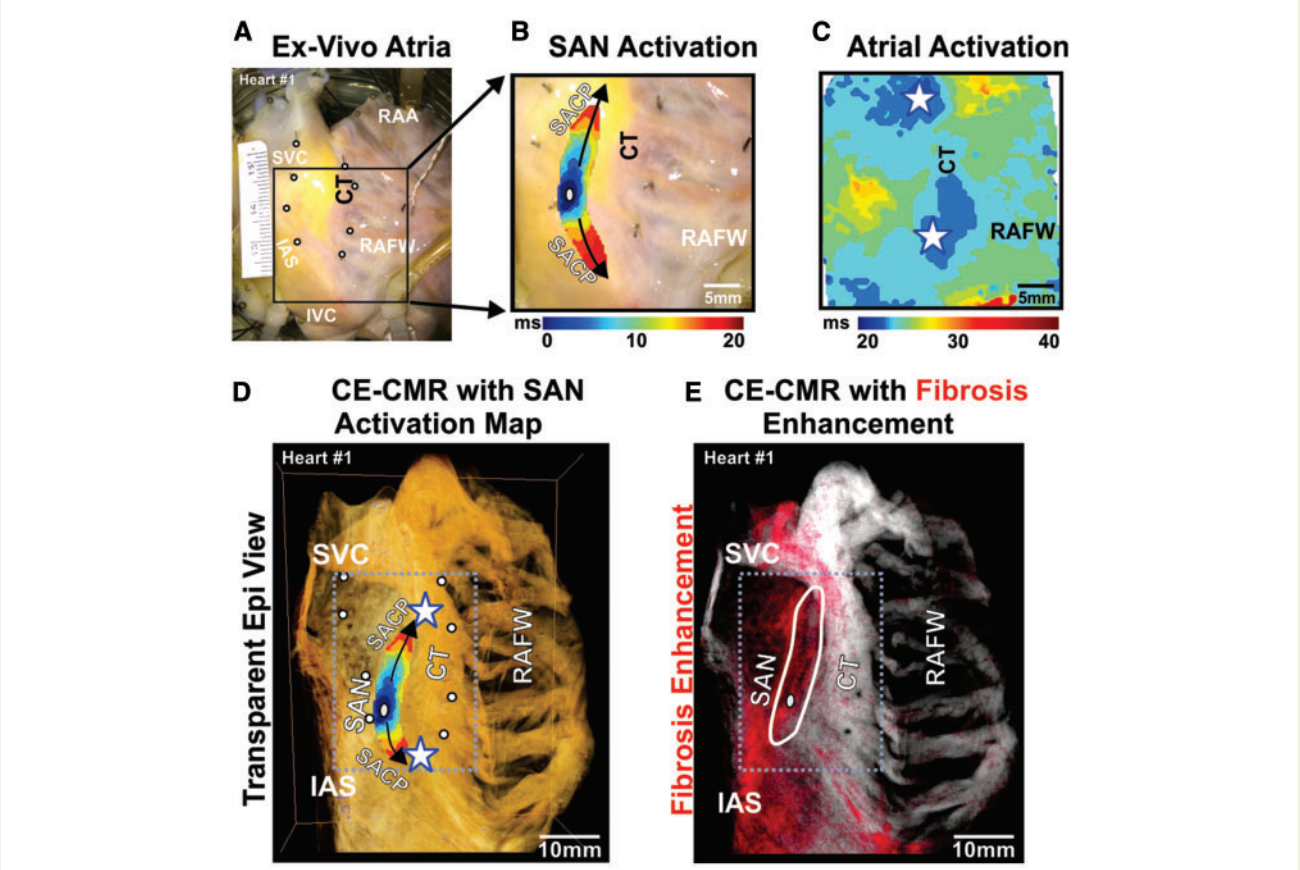

Figure 4 Human SAN pacemaker structure identified by optical mapping and CE-CMR *ex vivo*. (*A*) Photo of right atrial preparation (Heart 1) with optical field of view. White circles show location of pins, inserted after the functional experiment, which were used to correlate SAN function to SAN structure. (*B*) SAN activation map showing activation from SAN leading pacemaker (grey oval) superiorly and inferiorly to atrial breakthrough points (stars) at SAN conduction pathways connecting the SAN to the atria (black arrows). (*C*) Epicardial atrial activation showing atrial breakthrough points (stars). (*D*) CE-CMR of the RA overlapped with SAN activation map (atrial breakthrough denoted by white stars). Accurate overlap of SAN activation was done by locating holes in the preparation from the pins (white circles). (*E*) CE-CMR of RA with red fibrosis enhancement mask showing increased fibrosis in the intercaval region including SAN area (outlined in white). CT, crista terminalis; IAS, interatrial septum; IVC, inferior vena cava; RAA, right atrial appendages; RAFW, right atrial free wall; SACP, sinoatrial node conduction pathway; SAN, sinoatrial node.

of the SAN was more distinguishable than the SAN tail, which blended with the fibrotic IAS inferiorly. A signal intensity threshold of 2–3 SD (2.7 ± 0.5 SD) was found to accurately emulate SAN location and fibrotic content from *ex vivo* studies. The SAN region was delineated from surrounding atrial regions by its greater fibrosis density and was visualized in 10–15 LGE-CMR sections (*Figure 3*). The delineation of the medial SAN border was not always distinct due to the presence of fibrosis in SVC and IAS, which was consistent with *ex vivo* analysis. Thus, maximum SAN width was limited to 9 mm. The SAN region size, beginning from the septal boundary at the level of the right superior pulmonary vein to the superior junction of the SVC and RA, showed length, 23.6 ± 1.9 mm; width, 7.2 ± 0.9 mm; and depth, 2.9 ± 0.4 mm (see Supplementary data online, *Table S3*), which is in accordance with previous histological studies of the human SAN.[1,7–9] The SAN composed of 41.9 ± 5.4% LGE voxels above threshold compared with the RAFW (0.6 ± 0.6%, $P < 0.01$) and IAS (14.6 ± 5.0%, $P < 0.01$) (*Figure 5B* and *Table 1*). *Table 1* lists fibrosis quantification across the full range of thresholds analysed and which threshold was ultimately used for fibrosis quantification of each heart. Histograms showing atrial intensity used for regional fibrosis enhancement analysis of Volunteer 1A are shown in *Figure 2*.

Functional and histological identification of SAN pacemaker complex *ex vivo*

Near-infrared optical mapping revealed that all five coronary-perfused human SAN preparations exhibited stable sinus rhythm (83 ± 17 bpm) with the leading pacemaker site in the SAN fibrotic region (*Figure 4*). SAN activation preferentially travelled superiorly and/or inferiorly from the leading pacemaker before exiting the SAN through a preferential sinoatrial conduction pathway to excite the atria (*Figure 4C*), consistent with previous clinical[20] and experimental[5,6] observations. In all hearts, subsequent analysis of histological 2D sections of SAN and surrounding tissue delineated SAN pacemaker structure from surrounding tissue and confirmed that leading pacemaker locations were always within the fibrotic SAN structure (*Figure 5*).

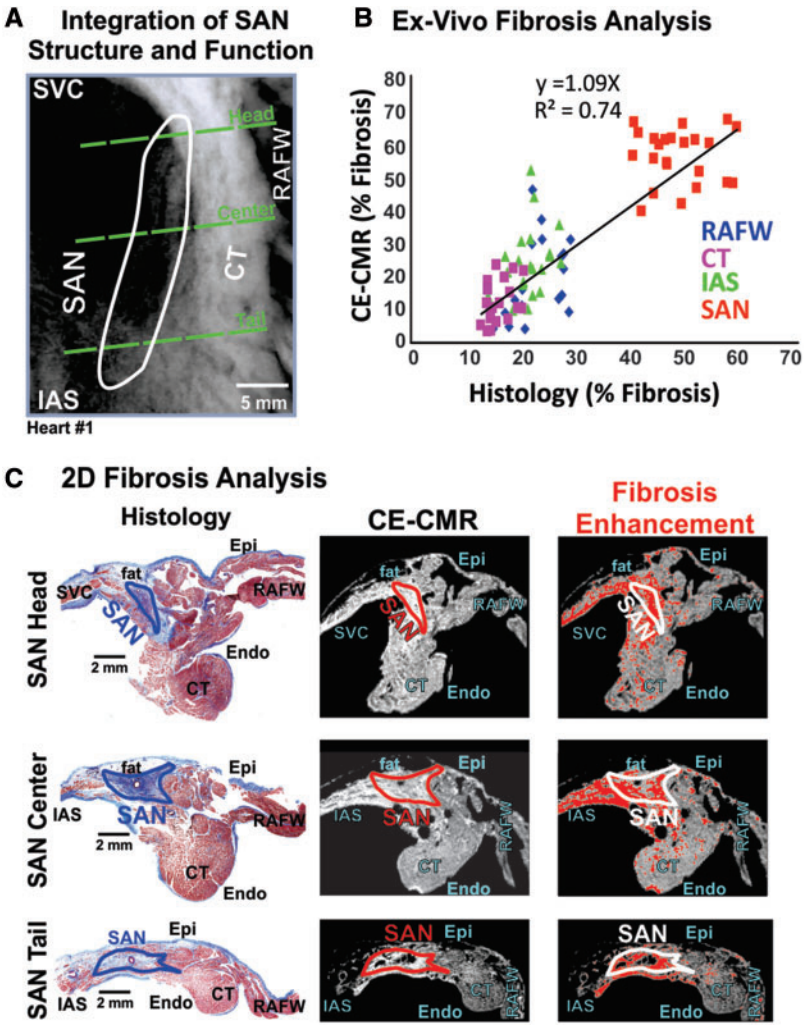

Figure 5 CE-CMR validated by histology for SAN fibrosis detection *ex vivo*. (*A*) CE-CMR overlapped with SAN border of Heart 1. Green dashed lines show SAN head, centre, and tail regions of 2D CE-CMR and histology sections. (*B*) 2D section *ex vivo* fibrosis analysis of SAN, IAS, RAFW, and CT by CE-CMR is strongly correlated with fibrosis analysis by histology. (*C*) Left: 2D histology images from the SAN head, centre, and tail showing distinct SAN fibrotic structure (blue) separated from atrial myocardium (red). Middle: 2D raw CE-CMR sections of the SAN head, centre, and tail. Right: The same CE-CMR 2D sections with a red fibrosis enhancement mask applied, showing increased fibrosis enhancement in the SAN region. CT, crista terminalis; Endo, endocardium; Epi, epicardium; IAS, interatrial septum; RAFW, right atrial free wall; SAN, sinoatrial node.

CE-CMR SAN fibrosis analysis of *ex vivo* atria

CE-CMR allowed for the delineation of the 3D SAN structure (*ex vivo*: length: 21.9 ± 4.3 mm, width: 4.4 ± 0.9 mm, depth: 2.2 ± 0.3 mm, see Supplementary data online, *Table S3*) by distinguishing a significant increase in fibrosis in SAN compared with surrounding atrial tissue in *ex vivo* hearts. Moreover, fibrosis analysis of the SAN, CT, RAFW, and IAS were strongly correlated ($r^2 = 0.74$, $P < 0.01$) between histology and 2D CE-CMR cross sections (*Figure 5B*). A sub-epicardial layer of fat was observed overlaying the SAN by histology, yet this same fat layer was supressed in the CE-CMR, which confirms fat supression and the specificity of enhancement for fibrosis (*Figure 5C*). Fibrosis threshold of signal intensity 0.8–1 SD above average RAFW signal was typically found to best match fibrosis analysis in histological images. Both regional 3D CE-CMR and histological analysis identified significantly greater fibrotic content in the SAN (46.0 ± 6.9% and 49.4 ± 3.1%, respectively) vs. other RA structures ($P < 0.05$); IAS (23.4 ± 15.7% (range: 4.8–47.6%) and 21.7 ± 2.0% (range: 19.7–25.4%); CT (28.5 ± 10.1% and 16.3 ± 2.4%), and RAFW (17.2 ± 6.9% and 23.3 ± 4.7%).

Discussion

For the first time, 3D human SAN fibrotic structure was visualized *in vivo* using LGE-CMR in five healthy volunteers. Fibrosis quantification and SAN identification by *in vivo* LGE-CMR were validated in

optically mapped explanted donor hearts by *ex vivo* contrast-enhanced CMR allied with serial histological sections of the SAN in the same *ex vivo* heart.

Rationale to utilize LGE-CMR to visualize human SAN fibrotic structure *in vivo*

LGE-CMR was originally proposed as a tool for visualizing[10] and quantifying[12] fibrotic scar tissue in the ventricle. This methodology was later applied for atrial fibrosis analysis *in vivo* by several groups.[11,13,21–24] Despite a significant number of recent LGE-CMR studies of the human atria,[11,13,21–24] most focus only on the LA, and no previous LGE-CMR study has defined or analysed SAN structure.[22] We hypothesized that *in vivo* visualization of SAN structure is possible with LGE-CMR due to the relatively large fibrotic content and size (~15 to 27 × 4 to 8 × 3 mm^3) of the human SAN.[1,7–9]

SAN structure has been identified as a major factor in normal SAN function and its macrostructural features, such as the SAN location, size, shape, and high percent of collagen tissue are generally accepted.[1,8,9] However, these SAN structural features have been studied by histological sectioning in *ex vivo* human SAN that are not possible to utilize *in vivo* to analyse the human SAN structure.

The ability to properly identify the SAN location may have important clinical implications, but current clinical electrophysiology approaches may be unable to do so.[25] Surface electrode mapping must rely on locating the earliest atrial activation, which may be 5–20 mm away from the intramural anatomic location of the SAN leading pacemaker due to the intramural 3D structure of the human SAN.[5,6] Thus, optical mapping is currently the only reliable method for localizing onset of activation within the SAN (*Figure 4*). However, as mentioned previously, optical mapping is limited to *ex vivo* experiments. An accurate knowledge of the patient-specific SAN location from LGE-CMR may help guide electrophysiologists and prevent permanent damage to the SAN and neurovascular inputs during atrial fibrillation ablation, SVC isolation, and atrial tachycardia ablation, thus reducing the risk of SAN dysfunction caused by ablation procedures.[26] Such accurate SAN imaging characterization may also increase the success rate of ablation of inappropriate sinus tachycardia and potentially enhance the understanding of this disorder as well as other forms of SAN dysfunction.

Ex vivo human studies provide proof-of-concept to visualize SAN structure with CMR

To provide proof-of-concept of CE-CMR to visualize 3D SAN structure, explanted human heart CE-CMR of optically mapped SAN was conducted. *Ex vivo* CE-CMR allows for increased resolution and the ability to histologically validate fibrosis analysis. Our laboratory's unique opportunity to study *ex vivo* human hearts allows us to utilize high-resolution functional and structural mapping, which is unavailable *in vivo*. Importantly, this combination of high-resolution structural-functional experiments was used to directly study the human heart, rather than animal models, which may contain relatively too little fibrotic tissue content[7] to visualize the SAN with CE-CMR.

In this study, *ex vivo* CE-CMR and histology fibrosis content analysis distinguished SAN structure based on increased fibrotic content compared with the surrounding RA. Importantly, SAN location identification from functional mapping, CE-CMR, and histology were all consistent (*Figure 5*). For this reason, we sought to apply LGE-CMR to define the 3D SAN structure *in vivo*.

In vivo LGE-CMR visualization of human SAN

Our *in vivo* LGE-CMR methodology has high enough resolution to visualize SAN structure. Given the in-plane resolution of the current *in vivo* LGE-CMR study (1 × 1 mm^2 for Volunteers 1–3 and 5; 0.65 × 0.65 mm^2 for Volunteer 4), the SAN structure with ~6 mm width and ~3 mm intramural thickness should be detectable in ~10 to 15 pixels of each 2D cross section. Additionally, the current slice thickness of our LGE-CMR is 1–1.25 mm and the SAN structure may extend superior/inferiorly 10–15 mm. Average SAN size in *ex vivo* CE-CMR and *in vivo* LGE-CMR were both within range of previous SAN structure studies *ex vivo* (~15 to 27 × 4 to 8 × 3 mm^3).[6,8,27]

While the superior and lateral LGE fibrotic borders of the SAN were distinct, the medial border tended to blend with SVC and IAS LGE fibrosis and was less distinct. The IAS contained high LGE, which was also seen in other LGE-CMR studies[22] and may be explained by the naturally high fibrotic content of this anatomic region.[27] Of note, LGE-CMR RA fibrosis values were less than RA regions of hearts analysed with *ex vivo* CE-CMR or *ex vivo* histology (*Figure 5* and *Table 1*). The resolution of LGE-CMR may account for the decreased values of fibrosis percent in these RA regions, as small interstitial fibrosis strands may be averaged with surrounding myocardium within a single voxel, thus decreasing the voxel's intensity below the threshold. Furthermore, any underlying cardiovascular disease in the *ex vivo* donor hearts could contribute to the slightly larger degree of fibrosis in the *ex vivo* hearts compared with our healthy volunteers.

Regional fibrosis analysis results from *in vivo* LGE-CMR, *ex vivo* CE-CMR, and histology of the SAN regions were all consistent. We found that *in vivo* LGE-CMR fibrosis analysis best reproduced our *ex vivo* (*Figure 5*) and previously reported histological values[6,9] when a threshold between 2 and 3 SD was chosen; moreover, in four of the LGE-CMR scans, a threshold of 3 SD was used to distinguish fibrosis while two of the LGE-CMR scans had a threshold of 2 SD. Importantly, the visualization of SAN fibrotic region, location, and size were not affected by the contrast agent used (*Figure 3* and see Supplementary data online, *Figure S1*), which is promising for the wide spread application of this technique, as contrast agents differ among CMR centres.

Future directions

Studies of a greater number and variety of both volunteers and patients should be done to establish baseline normal anatomy as well as age and gender-dependent normal values for healthy SAN. Additionally, further *in vivo* CMR studies are needed to understand whether there is a correlation between anatomic variations and SAN functional data as well as different types of SAN disease (exit block, chronotropic incompetence, and sinus arrest). Current clinical diagnosis of SAN dysfunction is hampered by functional tests with marginal sensitivity that provide no direct information of SAN structural remodelling, which is one of the major factors in SAN dysfunction.[28] Based on promising *ex vivo* studies of the human and animal SAN during SAN dysfunction, the consideration of patient-specific SAN

structure in the diagnosis of SAN dysfunction may be warranted. Thus, by using advanced 3D imaging techniques, clinical criteria for SAN dysfunction may include structural aspects, facilitating a better characterization of the disease. On the basis of this study, testing the utility of LGE-CMR to predict SAN function should be addressed in future studies.

Study limitations

The number of hearts studied, both *in vivo* and *ex vivo*, limit the extrapolation of our findings to wider populations. Furthermore, all LGE-CMR scans were done in healthy male hearts with no direct histological validation of fibrosis threshold. We did not study the SAN of structurally remodelled atria in patients with heart disease.

Conclusion and clinical applications

This is the first *in vivo* application of LGE-CMR to visualize and analyse 3D human SAN fibrotic structure. Visualization of SAN fibrotic structure may be used as a quality control test of future LGE-CMR studies of atrial fibrosis, as LGE-CMR scans unable to locate a region consisting of ~50% intramural fibrosis may not be able to reliably resolve atrial fibrosis. Furthermore, *in vivo* visualization of the human SAN structure with LGE-CMR may provide clinicians a new tool to avoid or target SAN structure during surgery or ablation and may benefit targeted therapeutics such as atrial pacing lead location or local gene/cell therapy delivery in the future.

Supplementary data

Supplementary data are available at *European Heart Journal - Cardiovascular Imaging* online.

Acknowledgements

We sincerely thank the Lifeline of Ohio Organ Procurement Organization and the Division of Cardiac Surgery at The OSU Wexner Medical Center for providing the explanted hearts: Mr Benjamin Canan and Eric Schultz for help with tissue processing and Ms Debbie Scandling for assistance with *in vivo* CMR scanning.

Conflict of interest: None declared.

Funding

This work was supported by NIH HL115580 and AHA GIA (V.V.F.), HL113084 (P.M.L.J.), HL084583, HL083422, HL114383 (P.J.M.), by funding from Dorothy M. Davis Heart and Lung Research Institute, OSU, and by National Heart Foundation of New Zealand (J.Z.).

References

1. James TN. Anatomy of the human sinus node. *Anat Rec* 1961;**141**:109–39.
2. Boyett MR, Honjo H, Kodama I. The sinoatrial node, a heterogeneous pacemaker structure. *Cardiovasc Res* 2000;**47**:658–87.
3. Keith A, Flack M. The form and nature of the muscular connections between the primary divisions of the vertebrate heart. *J Anat Physiol* 1907;**41**(Pt 3):172–89.
4. Boineau JP, Canavan TE, Schuessler RB, Cain ME, Corr PB, Cox JL. Demonstration of a widely distributed atrial pacemaker complex in the human heart. *Circulation* 1988;**77**:1221–37.
5. Fedorov VV, Glukhov AV, Chang R, Kostecki G, Aferol H, Hucker WJ *et al.* Optical mapping of the isolated coronary-perfused human sinus node. *J Am Coll Cardiol* 2010;**56**:1386–94.
6. Csepe TA, Zhao J, Hansen BJ, Li N, Sul LV, Lim P *et al.* Human sinoatrial node structure: 3D microanatomy of sinoatrial conduction pathways. *Prog Biophys Mol Biol* 2016;**120**:164–78.
7. Csepe TA, Kalyanasundaram A, Hansen BJ, Zhao J, Fedorov VV. Fibrosis: a structural modulator of sinoatrial node physiology and dysfunction. *Front Physiol* 2015;**6**:37.
8. Chandler N, Aslanidi O, Buckley D, Inada S, Birchall S, Atkinson A *et al.* Computer three-dimensional anatomical reconstruction of the human sinus node and a novel paranodal area. *Anat Rec (Hoboken)* 2011;**294**:970–9.
9. Shiraishi I, Takamatsu T, Minamikawa T, Onouchi Z, Fujita S. Quantitative histological analysis of the human sinoatrial node during growth and aging. *Circulation* 1992;**85**:2176–84.
10. Kim RJ, Fieno DS, Parrish TB, Harris K, Chen EL, Simonetti O *et al.* Relationship of MRI delayed contrast enhancement to irreversible injury, infarct age, and contractile function. *Circulation* 1999;**100**:1992–2002.
11. Oakes RS, Badger TJ, Kholmovski EG, Akoum N, Burgon NS, Fish EN *et al.* Detection and quantification of left atrial structural remodeling with delayed-enhancement magnetic resonance imaging in patients with atrial fibrillation. *Circulation* 2009;**119**:1758–67.
12. Scott PA, Morgan JM, Carroll N, Murday DC, Roberts PR, Peebles CR *et al.* The extent of left ventricular scar quantified by late gadolinium enhancement MRI is associated with spontaneous ventricular arrhythmias in patients with coronary artery disease and implantable cardioverter-defibrillators. *Circ Arrhythm Electrophysiol* 2011;**4**:324–30.
13. Spragg DD, Khurram I, Zimmerman SL, Yarmohammadi H, Barcelon B, Needleman M *et al.* Initial experience with magnetic resonance imaging of atrial scar and co-registration with electroanatomic voltage mapping during atrial fibrillation: success and limitations. *Heart Rhythm* 2012;**9**:2003–9.
14. Harrison JL, Jensen HK, Peel SA, Chiribiri A, Grondal AK, Bloch LO *et al.* Cardiac magnetic resonance and electroanatomical mapping of acute and chronic atrial ablation injury: a histological validation study. *Eur Heart J* 2014;**35**:1486–95.
15. Hansen BJ, Zhao J, Csepe TA, Moore BT, Li N, Jayne LA *et al.* Atrial fibrillation driven by micro-anatomic intramural re-entry revealed by simultaneous sub-epicardial and sub-endocardial optical mapping in explanted human hearts. *Eur Heart J* 2015;**36**:2390–401.
16. Lou Q, Hansen BJ, Fedorenko O, Csepe TA, Kalyanasundaram A, Li N *et al.* Upregulation of adenosine A1 receptors facilitates sinoatrial node dysfunction in chronic canine heart failure by exacerbating nodal conduction abnormalities revealed by novel dual-sided intramural optical mapping. *Circulation* 2014;**130**:315–24.
17. Fedorov VV, Schuessler RB, Hemphill M, Ambrosi CM, Chang R, Voloshina AS *et al.* Structural and functional evidence for discrete exit pathways that connect the canine sinoatrial node and atria. *Circ Res* 2009;**104**:915–23.
18. Fedorov VV, Glukhov AV, Chang R. Conduction barriers and pathways of the sinoatrial pacemaker complex: their role in normal rhythm and atrial arrhythmias. *Am J Physiol Heart Circ Physiol* 2012;**302**:H1773–83.
19. Joyner RW, van Capelle FJ. Propagation through electrically coupled cells. How a small SA node drives a large atrium. *Biophys J* 1986;**50**:1157–64.
20. Stiles MK, Brooks AG, Roberts-Thomson KC, Kuklik P, John B, Young GD *et al.* High-density mapping of the sinus node in humans: role of preferential pathways and the effect of remodeling. *J Cardiovasc Electrophysiol* 2010;**21**:532–9.
21. McGann C, Akoum N, Patel A, Kholmovski E, Revelo P, Damal K *et al.* Atrial fibrillation ablation outcome is predicted by left atrial remodeling on MRI. *Circ Arrhythm Electrophysiol* 2014;**7**:23–30.
22. Akoum N, McGann C, Vergara G, Badger T, Ranjan R, Mahnkopf C *et al.* Atrial fibrosis quantified using late gadolinium enhancement MRI is associated with sinus node dysfunction requiring pacemaker implant. *J Cardiovasc Electrophysiol* 2012;**23**:44–50.
23. Khurram IM, Habibi M, Gucuk IE, Chrispin J, Yang E, Fukumoto K *et al.* Left atrial LGE and arrhythmia recurrence following pulmonary vein isolation for paroxysmal and persistent AF. *JACC Cardiovasc Imaging* 2016;**9**:142–8.
24. Chrispin J, Gucuk IE, Zahid S, Prakosa A, Habibi M, Spragg D *et al.* Lack of regional association between atrial late gadolinium enhancement on cardiac magnetic resonance and atrial fibrillation rotors. *Heart Rhythm* 2016;**13**:654–60.
25. Jacobson JT, Kraus A, Lee R, Goldberger JJ. Epicardial/endocardial sinus node ablation after failed endocardial ablation for the treatment of inappropriate sinus tachycardia. *J Cardiovasc Electrophysiol* 2014;**25**:236–41.
26. Kitamura T, Fukamizu S, Arai K, Hojo R, Aoyama Y, Komiyama K *et al.* Transient sinus node dysfunction following sinus node artery occlusion due to radiofrequency catheter ablation of the septal superior vena cava-right atrium junction. *J Electrocardiol* 2016;**49**:18–22.
27. Sanchez-Quintana D, Cabrera JA, Farre J, Climent V, Anderson RH, Ho SY. Sinus node revisited in the era of electroanatomical mapping and catheter ablation. *Heart* 2005;**91**:189–94.
28. Mangrum JM, DiMarco JP. The evaluation and management of bradycardia. *N Engl J Med* 2000;**342**:703–9.